Acta Biomaterialia 34 (2016) 41–52

Contents lists available at ScienceDirect

Acta Biomaterialia

journal homepage: www.elsevier.com/locate/actabiomat

Full length article

Synergistic influence of collagen I and BMP 2 drives osteogenic differentiation of mesenchymal stem cells: A cell microarray analysis ☆

Soraya Rasi Ghaemi [a], Bahman Delalat [a], Xavier Cetó [a], Frances J. Harding [a], Jonathan Tuke [b], Nicolas H. Voelcker [a,*]

[a] ARC Centre of Excellence in Convergent Bio-Nano Science and Technology, Mawson Institute, University of South Australia, South Australia, Australia
[b] School of Mathematical Sciences, University of Adelaide, South Australia, Australia

ARTICLE INFO

Article history:
Received 26 March 2015
Received in revised form 5 June 2015
Accepted 17 July 2015
Available online 18 July 2015

Keywords:
High throughput screening
MSC differentiation
Osteogenesis
Collagen I
Bone morphogenetic protein 2

ABSTRACT

Cell microarrays are a novel platform for the high throughput discovery of new biomaterials. By re-creating a multitude of cell microenvironments on a single slide, this approach can identify the optimal surface composition to drive a desired cell response. To systematically study the effects of molecular microenvironments on stem cell fate, we designed a cell microarray based on parallel exposure of mesenchymal stem cells (MSCs) to surface-immobilised collagen I (Coll I) and bone morphogenetic protein 2 (BMP 2). This was achieved by means of a reactive coating on a slide surface, enabling the covalent anchoring of Coll I and BMP 2 as microscale spots printed by a robotic contact printer. The surface between the printed protein spots was passivated using poly (ethylene glycol) bisamine 10,000 Da (A-PEG). MSCs were then captured and cultured on array spots composed of binary mixtures of Coll I and BMP 2, followed by automated image acquisition and quantitative, multi-parameter analysis of cellular responses. Surface compositions that gave the highest osteogenic differentiation were determined using Runx2 expression and calcium deposition. Quantitative single cell analysis revealed subtle concentration-dependent effects of surface-immobilised proteins on the extent of osteogenic differentiation obscured using conventional analysis. In particular, the synergistic interaction of Coll I and BMP 2 in supporting osteogenic differentiation was confirmed. Our studies demonstrate the value of cell microarray platforms to decipher the combinatorial interactions at play in stem cell niche microenvironments.

1. Introduction

The application of stem cells to regenerative medicine has created a strong demand for culture constructs able to regulate cellular response. In this context, experimental platforms that can capture the multiplicity of factors, and their combinations, at play within the stem cell niche environment are required. Concurrently, the systems biology field is progressing toward high-content/high-throughput discovery, facilitating the multiplexed analysis of environmental parameters. Together, these developments have driven the fabrication of miniaturised bioassay platforms compatible with long-term tissue culture, and thus suitable for the investigation of stem cell differentiation [1,2]. In this study, we use the protein microarray format to investigate the effect of surface-immobilised proteins on osteogenic differentiation of mesenchymal stem cells (MSCs) [3]. The regulation of MSC differentiation *via* biomaterial surfaces would translate into advances in regenerative medicine [4–6].

The differentiation of multipotent MSCs into osteogenic cells depends on the spatially coordinated activities of multiple signalling pathways that include growth factors (GFs) and extracellular matrix (ECM) components [7–9]. Considerable attention has been devoted to extrinsic factors that orchestrate determination and differentiation of MSCs [10–14]. Many soluble signals and insoluble cues known to stimulate MSC differentiation to osteogenic cells have already been identified, including dexamethasone [15,16], BMP 2 [17–19], vitronectin and Coll I [10,20]. The response to these signals is biphasic: a response is triggered only when a factor is present above a certain threshold concentration [7]. However, it is not straightforward to convert this knowledge into directed differentiation of MSC *in vivo* [21]. For example, dexamethasone prompts osteoblast differentiation of MSC *in vitro*, but is reported to hinder bone growth *in vivo* [22], which limits its

☆ Part of the High Throughput Approaches to Screening Biomaterials Special Issue, edited by Kristopher Kilian and Prabhas Moghe.

* Corresponding author.
E-mail addresses: soraya.rasi_ghaemi@mymail.unisa.edu.au (S. Rasi Ghaemi), Bahman.Delalat@unisa.edu.au (B. Delalat), Xavier.CetoAlseda@unisa.edu.au (X. Cetó), Fran.Harding@unisa.edu.au (F.J. Harding), simon.tuke@adelaide.edu.au (J. Tuke), Nico.Voelcker@unisa.edu.au (N.H. Voelcker).

http://dx.doi.org/10.1016/j.actbio.2015.07.027
1742-7061/

use in bone regeneration. In order to control MSC behaviour more precisely and hence develop fit-for-clinical-purpose technology, scaffolds presenting GF and ECM proteins or derivative peptides have been designed.

MSC are particularly responsive to extracellular matrix (ECM) proteins. Collagen I (Coll I) [23,24] and derivative peptides [25] incorporated into scaffolds are documented to drive osteogenic differentiation of MSC. MSCs even establish a Coll I containing ECM protein layer before they undergo osteoblastic differentiation and express osteoblast-related genes [26,27], suggesting that the ECM environment plays a crucial role in this differentiation pathway. Insoluble cues such as Coll I influence cellular differentiation through unique integrin-mediated signalling mechanisms [28]. Clinically, absorbable collagen sponges are used for the delivery of BMP 2 to fracture and defect sites to promote bone repair [9,10,29,30]. BMP 2 is known to induce osteogenic differentiation through interactions with its specific receptors. BMP 2 protein regulates osteoblast gene expression by up-regulating transcription factors Runx2 and Osterix [31]. Synergy between the osteopromotive effects of Coll I and BMP 2 appears active from the early stages of osteoblast differentiation [32] through to bone mineralisation, with integrin signalling supplied by Coll I regulating cell response to BMP 2. There are indications that the combined influence of Coll I and BMP 2 may extend even earlier back to the initial osteogenic commitment from MSC [10,32].

We therefore hypothesised that co-immobilisation of both BMP 2 and Coll I onto a scaffold surface will accelerate MSC osteogenesis. To investigate the influence of combinatorial surface-immobilised Coll I and BMP 2, we developed an experimental paradigm that is based on parallel, *in vitro* exposure of MSCs to a diverse array of defined extracellular signals presented individually and in combination. The ultimate goal of our study was to identify the optimum ratio of Coll I and BMP 2 that serves to induce the differentiation of MSCs to the osteogenic cell lineage.

2. Materials and methods

2.1. Fabrication of microarray platforms

Prior to silanisation, glass microscopy slides were pre-cleaned by rinsing in 70% ethanol and Milli-Q water, followed by treatment with Piranha solution (40% H_2SO_4 and 60% H_2O_2) at room temperature for 60 min. After washing slides with Milli-Q water and drying with compressed nitrogen, the samples were dip-coated in a 10% solution of the epoxy silane (3-glycidyloxypropyl) trimethoxysilane (GOPTMS) (Sigma Aldrich) in dry toluene at room temperature for 30 min [3,33]. Excessive GOPTMS was removed by rinsing with dry toluene subsequently, samples were dried in a stream of dry nitrogen gas. This base coating provided terminal epoxy-functional groups suitable for the covalent anchoring of amine groups of arrayed proteins and A-PEG passivating agents (Fig. 1).

Proteins were printed on freshly epoxy-silane-coated slides using a XactII™ Compact Microarray System equipped with 750 µm diameter Xtend™ Capillary Microarray Pins. In order to study MSC differentiation to osteogenic lineages, defined combinations of Coll I (Millipore) at concentrations of 50, 100, 200 µg/mL and BMP 2 (Abcam) at concentrations of 1, 5, 10, 20, and 50 µg/mL were prepared in a 384-well plate (MJ Research) to a final volume of 50 µL.

The proteins to be printed were diluted in sterile Dulbecco's phosphate-buffered saline solution (PBS) at pH 5. PBS was adjusted to pH 5 with glacial acetic acid to prevent gelling and precipitation of collagen and to increase the solubility of the lyophilised BMP 2. Glycerol was added to each protein solution at final concentration of 2% [3,34]. Proteins were spotted under conditions of 65% humidity and 11 °C. After printing, arrays were stored at 4 °C for 12 h. To impede non-specific protein adsorption and cell attachment between arrayed protein spots, the non-printed area was passivated by A-PEG 10,000 Da (Sigma Aldrich) under cloud-point conditions for 12 h. A-PEG at a concentration of 10 mg/mL was dissolved in 0.1 M phosphate buffer at pH 6.5 containing K_2SO_4 at a concentration of 0.75 M.

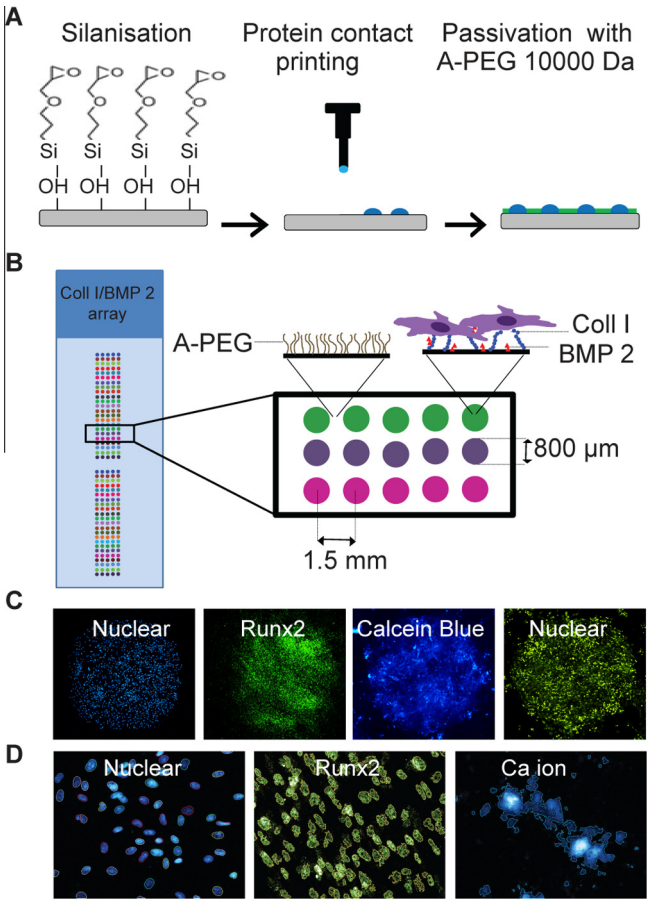

Fig. 1. Schematic of cell microarray formation: (A) glass slides were coated with GOPTMS, yielding an epoxy-terminated surface. Arrays of pre-mixed combinations of Coll I and BMP 2 printing solutions were fabricated using a contact microarrayer. Subsequently, A-PEG was grafted on the slide surface by covalent attachment to epoxy groups. (B) A typical cell microarray platform with various ratios of Coll I and BMP 2 printed on the epoxy-modified slide. Each factor combination was printed in ten replicates on the one slide. (C) Fluorescence images of the entire slide were acquired at two excitation wavelengths (excitation ~480 nm, emission ~520 nm for the green channel and excitation ~343 nm, emission ~483 nm for the blue channel) using an automated high content fluorescence microscopy. (D) Automated analysis: for cell counting purposes, each nucleus (Hoechst 33342 or PicoGreen stained) was detected as an object representing a cell. Runx2 positive cells in the green fluorescence channel were identified by the software (yellow outline). Calcium phosphate deposits (Calcein Blue staining) are indicated by the blue outline. (For interpretation of the references to colour in this figure legend, the reader is referred to the web version of this article.)

2.2. Surface characterisation

Water contact angle measurements were conducted on silanised clean glass slides and on Piranha-treated glass as a control. Immediately after silanisation, 3 µL Milli-Q water drops were formed at a constant rate by motor-driven 100 µL Hamilton syringe and the images were captured using a Panasonic WV-BP550/G CCTV camera. The static contact angle was measured using ImageJ software (NIH) with the Drop Analysis plugin. Five points along the surface were evaluated in triplicate and the results averaged.

Protein immobilisation and A-PEG grafting on to the array surface were studied using XPS and ToF-SIMS. XPS analysis was carried out on an ultrahigh vacuum apparatus equipped with a nonmonochromatic Mg and Al Kα source. The total pressure in the main vacuum was 5×10^{-9} mbar during analysis. The spectra of the electrons emitted from the samples surface were recorded with a hemispherical Phoibos 100 energy analyser from SPECS. The measurement angle between the X-ray irradiation and the analyser was 54°. A Mg Kα source at an anode voltage of 12 kV and emission current of 100 W was used to acquire XPS spectra. Survey scans were performed at a pass energy of 40 eV. Atomic concentrations were calculated from the spectrum peak areas using Casa XPS program version 2.3.10 (Casa Software). High resolution C1S spectra were recorded in 0.05 eV steps with a pass energy of 40 eV. The binding energy peaks were deconvoluted using a Simplex algorithm to determine optimised curve fits and the contributions from specific functional groups. ToF-SIMS experiments were performed using aPHI TRIFT V nanoToF instrument (Physical Electronics Inc.), equipped with a pulsed liquid metal $69Au^+$ primary ion gun. This was operated at 30 kV energy. A spectral range up to 1850 *m*/*z* was acquired, but only peaks in the low mass range below 500 *m*/*z* were used for analysis. Chemical maps of eight amino acid ions associated with Coll I and BMP 2 structure [35,36] and four ion fragments characteristic of A-PEG [37,38] were prepared to investigate the spatial distribution of these species. These peaks were reported as distinguishing spectral features associated with specific amino acid residues. The analysis protocol involved the analysis of 3 protein spots on each of 3 samples. Secondary ions were sampled from a $350 \times 350\ \mu m^2$ area of each protein spot. Sample spectra and images were processed by WincadenceN software (Physical Electronics Inc.).

The level of Coll I and BMP 2 immobilisation was also verified by immunofluorescence (IF) staining. After construction and passivation, the arrays were washed with PBS for 1 h to remove non-immobilised proteins and were blocked by 10% serum of the species that the secondary antibody was raised in for 30 min. Then the samples were incubated with a primary anti-BMP 2 IgG (1/100, Santa Cruz Biotechnology Q) antibody for 12 h at 4 °C. The arrays were subsequently incubated with the FITC-labelled and PE-labelled secondary antibody (1/200, Santa Cruz Biotechnology Inc.) in PBS including 1% BSA for 1 h in the dark. Samples were imaged using a fluorescence microscope (Nikon Eclipse 50i). Incubation of the arrayed platform with secondary antibody alone during the process of IF staining served as a control.

2.3. Bone marrow MSC isolation and culture

Rat MSCs were obtained from the bone marrow of 6–7 week old Wistar rats with a body weight of approximately 100 g (from Animal Care Unit, SA Pathology). MSCs were harvested with ethics approval by the SA Pathology Animal Ethics Committee. Bone marrow was collected by flushing femurs and tibias with Dulbecco's modified Eagle medium (DMEM-high glucose) (Sigma Aldrich) supplemented with 10% fetal bovine serum (FBS), 2 mM L-glutamine, 100 U/mL penicillin, and 0.1 mM nonessential amino acids (Sigma Aldrich) [12,39]. After filtration of cells through a nylon mesh filter with pore size of 100 μm (BD Falcon) and washing in medium, cells were treated with RBC lysis buffer (0.15 M NH_4Cl, 10 mM $KHCO_3$, 0.1 mM EDTA) for 5 min. Subsequently, cells were washed with medium and resuspended in DMEM supplemented with 10% FBS then incubated at 37 °C under 5% CO_2. Early passaged cells (passages 3–4) were used exclusively.

Prior to incubation with cells, microarray slides were washed with copious amounts of sterile PBS for 1 h to remove any excess and non-covalently bound biomolecules. The samples were sterilised by incubation in 200 U/mL penicillin (Invitrogen), 200 μg/mL streptomycin (Invitrogen), and 500 ng/mL amphotericin B (Invitrogen) in sterile PBS for 4 h. Each slide was placed in a four-well plate (Nunc) and seeded with MSCs at a density of 15,000 cells/cm^2. Cells were then incubated in contact with arrays for an incubation time of 30 min with DMEM medium without FBS at 37 °C and 5% CO_2. Loosely attached cells were then removed by washing with prewarmed culture medium. The cells were subsequently incubated in fresh medium including 10% FBS for 48 h. The medium was exchanged with osteogenic differentiation medium (Invitrogen). Half the medium volume was exchanged with fresh medium every 2 days. As biochemical markers of differentiation, we measured Runx2 expression after 6 days in culture and calcium phosphate deposition on the cell layer after 21 days in culture.

Differences in cell responses to external stimuli are known to be cell passage number dependent [40,41]. We eliminated these sources of variations by using cells from passages 3–4 for all experiments.

2.4. Assays for osteogenesis

To reveal Runx2 expression through IF, MSCs on the arrayed protein spots were washed with PBS and fixed with 4% paraformaldehyde solution (Sigma Aldrich) in PBS. Cells were then permeabilised with 0.25% Triton X-100 (Sigma Aldrich) for 5 min at room temperature. After washing with sterile PBS without Ca^{2+} and Mg^{2+}, cells were treated with a blocking solution of 10% serum obtained from the species that the secondary antibody was raised in, for 30 min to block unspecific binding sites. Samples then were incubated with mouse monoclonal anti-Rux2 IgG2b (1:200, Abcam) primary antibody at 4 °C overnight. Following three washes with PBS, arrays were incubated for 1 h (room temperature) with FITC conjugated rabbit anti-mouse IgG2b (1/100, Abcam) antibody. Cells were counterstained with Hoechst 33342 at a final concentration of 2 μg/mL for 15 min. Incubation of cells with secondary antibody without primary antibody against Runx2 in the process of IF staining served as a control.

The presence of mineralised nodules was confirmed by Calcein Blue staining. Calcein Blue powder (Sigma Aldrich) was dissolved in 100 mM KOH at the concentration of 30 mM and then filtered. Calcein Blue solution was added to medium to a final concentration of 30 μM. The cells were then incubated with Calcein Blue dye for 12 h. Counterstaining was performed by incubation of sample with 10 μM Pico Green (Invitrogen TM) for 10 min to quantify cell population on the spot.

Calcium phosphate deposition was also visualised by Alizarin Red staining in brightfield mode. Cells were fixed with 4% paraformaldehyde as described above, then incubated with 20 mg/mL Alizarin Red (Sigma Aldrich) solution for 20 min. Alizarin Red solution was prepared in Milli-Q water at a concentration of 20 mg/mL, and the pH was adjusted to 4.1–4.3 using 0.5% aqueous NH_4OH. The stained mineral nodules were visualised by means of brightfield microscopy (Nikon Eclipse Ti).

2.5. Imaging and data analysis

Fluorescently labelled cells on the arrays were imaged through a coverslip using the fully automated fluorescence microscopy Operetta™ (PerkinElmer). The system was programmed to scan each spot on the array. Image acquisition was controlled within the Harmony software environment (Perkin Elmer). For Runx2 expression analysis, channels with excitation ~480 nm, emission ~520 nm for the green channel and excitation ~343 nm, emission ~483 nm for the blue channel were used to acquire the images. Feature extraction was performed using analysis scripts that

employ built-in segmentation algorithms. The nuclear outlines of all cells were determined with a "find nuclei building block" using the nuclear stained images. Runx2 positive cells in a spot were detected using the IF staining against Runx2. The "calculate intensity property" was used to determine the intensity of stained Runx2 in the nuclear region (Fig. 1D). The colour intensity in every spot was normalised by cell number obtained by dividing the integral colour intensity in the spot by total number of cells in the same spot. The Runx2 staining intensities were also used to analyse the extent of differentiation in individual cells.

The area of deposited calcium phosphate in every spot was used to analyse late stage MSC differentiation [42]. The calcium phosphate deposited areas were quantified with a "Find Image Area" building block using Calcein Blue staining (Fig. 1D). Direction of differentiation was defined as the ratio of all calcium phosphate deposited areas and total cell number on the same spot.

2.6. Statistical analysis

Principal component analysis (PCA) was used to interpret the ToF-SIMS through images, by using specific routines written by the authors in Matlab 7.10 (MathWorks, Natick, MA). For data analysis, integrated peak data (peak areas) was first normalised to the total selected spectral counts to correct for differences in the total secondary ion intensity between experiments and samples, and afterwards mean-centred. In this way, the peak file used for PCA contained a total of 122 peaks in the form C_xH_y, $C_xH_yO_z$, $C_xH_yN_z$ and C_xH_yNO; neglecting any inorganic signal (e.g. Na, K or Si) or associated peaks. Additionally, 95% confidence ellipses were calculated for each of the groups of samples according to Wagner et al. [43].

A non-parametric ANOVA followed by a Tukey posthoc test was used to determine the significance of differences between the numbers of cell attached on microarray spots and calcium phosphate deposited areas.

To analyse Runx2 expression, modelling was performed in R (R core 2013). Examination of boxplots of Runx2 expression against Coll I and BMP 2 printing solution concentration indicated a sigmoidal relationship with BMP 2 and a linear relationship with Coll I. The response variable, Runx2, was regressed on the main predictors of Coll I and BMP 2 with up to cubic terms for BMP 2 to accommodate the sigmoidal relationship and linear terms for Coll I. Two-way interaction terms were also included. To test if any of these terms could be removed from the model; a step-down model selection technique was utilised with the Akaike's Information Criterion (AIC) as the measure of model fit. The AIC uses the likelihood as a measure of fit with a penalty term for the number of parameters in the model. It ensures the most parsimonious model. The step down procedure was achieved using the stepAIC function from the MASS library [44] in R. The final model was:

$$\mathrm{Runx2} \sim \mathrm{BMP} + \mathrm{BMP}^2 + \mathrm{BMP}^3 + \mathrm{Coll} + \mathrm{Coll} : \mathrm{BMP} + \mathrm{Coll} : \mathrm{BMP}^2 + \mathrm{Coll} : \mathrm{BMP}^3$$

Predictions from the model with 95% confidence intervals were then calculated and are shown in the results section. This suggests a regression model incorporating a cubic term for BMP 2 concentration:

$$\mathrm{Runx2} \sim \mathrm{f}(\mathrm{BMP}, (\mathrm{BMP}^2, \mathrm{BMP}^3, \mathrm{Coll}))$$

Residual analysis confirms that the fit of the model to the data is suitable for evaluation of Runx2 expression in the range of interest for surface optimisation.

3. Results

3.1. Fabrication of the microarray platforms

A contact microarrayer was used to print Coll I and BMP 2 and combinations of the two biomolecules on surface-modified glass slides, creating an array of 'molecular microenvironments', each comprising a defined mixture of the two signalling molecules (ESI† Fig. S1). To facilitate covalent immobilisation of each of the printed combinations, cleaned glass slides were coated with GOPTMS to present reactive epoxy groups on the surface. Those epoxy groups allowed the covalent anchorage of first printed proteins and subsequently A-PEG 10,000 Da (Fig. 1).

A silanisation time of 30 min resulted in an increase in surface contact angle to 59 ± 1.75° compared to a contact angle of the clean glass surface of around 12 ± 1.5° (ESI† Fig. S2A). Using Coll I, successful protein immobilisation on the epoxy-coated surface was confirmed by XPS. Whilst the XPS survey spectrum did not show a nitrogen peak on the epoxy-coated surface (ESI† Fig. S2B), a nitrogen signal of 5–8 atomic percentage (at.%) was present on Coll I printed spots (ESI† Fig. S2C). As expected, the observed signal increased with increasing Coll I printed formulation concentration from 50 to 200 μg/mL (Table S1). XPS C1s spectra provided information about the A-PEG grafting on the epoxy-coated surface (ESI† Fig. S3). A distinct increase in the C–O subpeak (at 286.5 eV) was observed when A-PEG was grafted onto the epoxy-coated slide (ESI† Fig. S3).

Time-of-flight secondary ion mass spectrometry (ToF-SIMS) was also used to corroborate the presence of protein on the printed spots. This analysis was performed for immobilised Coll I (100 μg/mL printed formulation concentration) and BMP 2 (50 μg/mL printed formulation concentration) and a mixture of Coll I and BMP 2 after passivation with A-PEG. ToF-SIMS spectra were acquired from within Coll I printed spots and Coll I/BMP 2 printed spots and ion distribution maps of the spot were also obtained [45]. Eight amino acid fragments derived from Coll I and BMP 2 [35,36] were detected (Table 1), in addition to four ion fragments of $C_2H_3O^+$, $C_2H_5O^+$, $C_3H_7O^+$ and CH_3O^+ characteristic of A-PEG, were identified by the ToF-SIMS.

The images obtained for typical Coll I, BMP 2 and Coll I/BMP 2 printed spot showed clearly defined round spots with a uniform surface coverage of all amino acid fragments assayed (Fig. 2). The $C_xH_yO^+$ ion image was chosen to map the distribution of A-PEG (Fig 2B) and the ion fragments of A-PEG distributed between the spots. Ion distribution maps show a decrease in detected $C_2H_5O^+$ ion density inside the printed spot, representative of the presence of A-PEG, with increasing printed formulation concentration (ESI† Fig. S5). The PCA score plot is shown in Fig. 3, where PC1 and PC2 account for 85.5% of the variance. With this analysis BMP 2 printed spots, Coll I printed spots and BMP 2/Coll I spots can be discriminated into different clusters, further confirmed through the plotting of the 95% confidence interval ellipses. Notably, the BMP 2/Coll I spots lie approximately in between and equidistant from

Table 1
List of the most prominent positive secondary ions on Coll I and BMP 2 printed spots after ToF-SIMS analysis.

Amino acid	Ion fragment
Alanine	$C_2H_6N^+$
Glutamine	$C_4H_6NO^+$
Hydroxyproline	$C_4H_8NO^+$
Leucine	$C_5H_{12}N^+$
Histidine	$C_4H_6N_2^+$
Proline	$C_4H_6N^+$
Lysine	$C_5H_{10}N^+$
Glycine	CH_4N^+

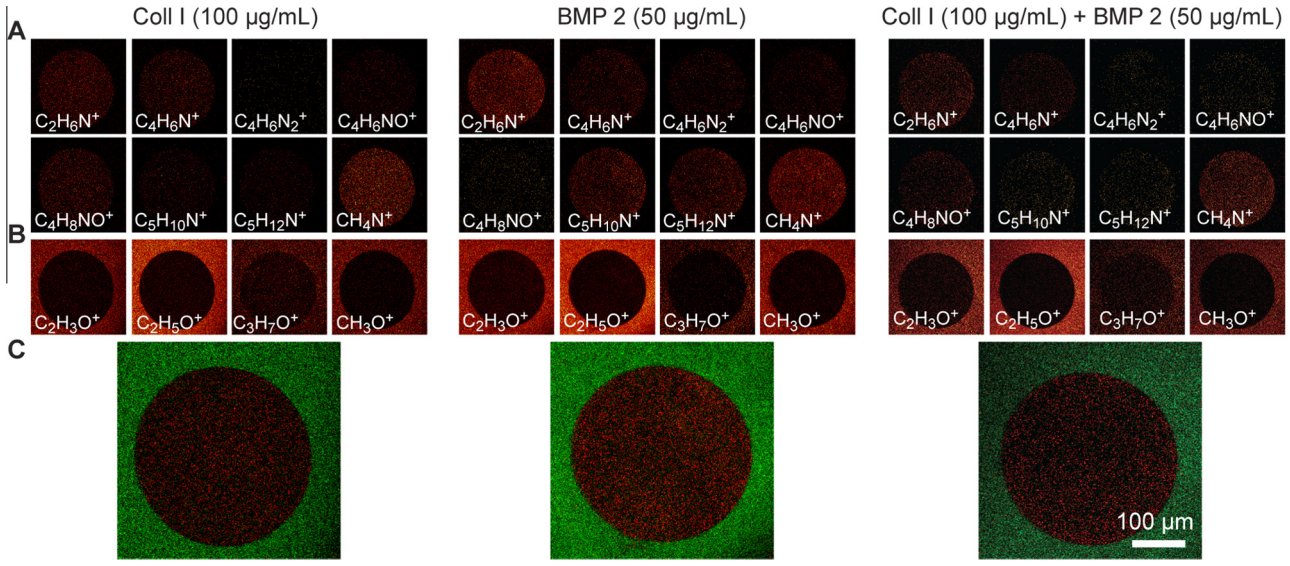

Fig. 2. ToF-SIMS ion maps of protein microarray spots: (A) ToF-SIMS imaging of regions within the printed array, showing ion maps for several amino acid residues contained within Coll I spots printed using formulation concentrations of 100 μg/mL, BMP 2 spots printed using formulation concentrations of 50 μg/mL and spots printed with Coll I and BMP 2 in combination on epoxy-coated slides (after passivation with A-PEG). (B) Ion mapping of C_xH_yO+ ion fragments for the same regions of the arrays shown in A, verifying A-PEG passivation of the un-printed array surface. (C) ToF-SIMS imaging showing an overlay of amino acid signal map (red) and A-PEG signal map (green). (For interpretation of the references to colour in this figure legend, the reader is referred to the web version of this article.)

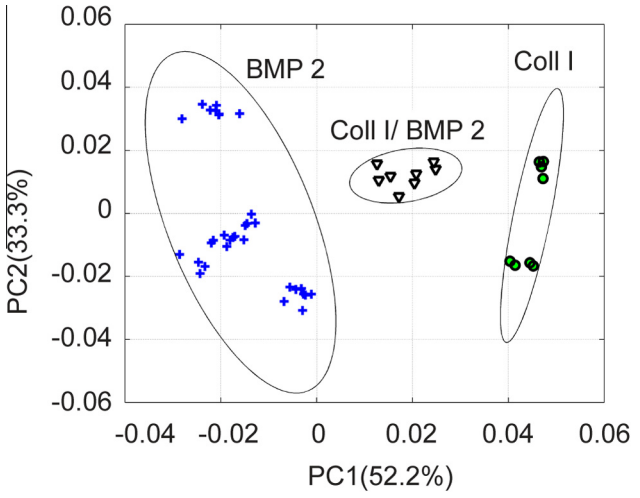

Fig. 3. Score plot of the first two components obtained after PCA analysis of the ToF-SIMS surface immobilised protein data: (+) BMP 2 printed with a solution concentration of 50 μg/mL, (●) Coll I printed with a solution concentration of 100 μg/mL and (▼) their combination. Additionally, 95% confidence ellipses for each of the groups are plotted.

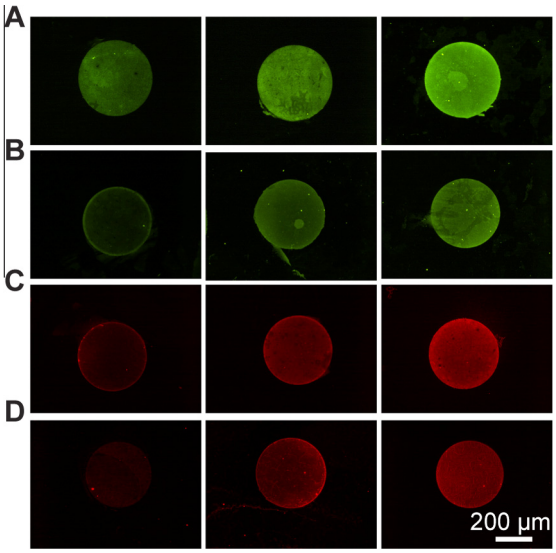

Fig. 4. IF staining of protein printed spots on epoxy-coated slide after passivation with A-PEG (12 h reaction time): (A) IF staining image of Coll I spots printed using formulation concentrations of 50, 100 and 200 μg/mL (green) from left to right, respectively. (B) IF staining of Coll I printed using formulation concentrations of 50, 100 and 200 μg/mL in combination with BMP 2 at a printed formulation concentration of 20 μg/mL from left to right, respectively. (C) IF staining of BMP 2 spots printed using formulation concentration s of 10, 20 and 50 μg/mL (red) from left to right, respectively. (D) IF staining of BMP 2 printed using formulation concentrations of 10, 20 and 50 μg/mL in combination with Coll I at a printed formulation concentration of 200 μg/mL from left to right, respectively. (For interpretation of the references to colour in this figure legend, the reader is referred to the web version of this article.)

BMP 2 and Coll I sample populations, indicating the creation of new surface chemistry when the two proteins are printed in combination. Examination of the respective loading plots for PC1 (ESI† Fig. S4) reveals that this separation is mainly due to $C_3H_5^+$, $C_2H_5^+$, $C_3H_7^+$, $C_4H_7^+$ and $C_4H_{10}N^+$ for BMP 2, and $C_4H_8N^+$ and CH_4N^+ for Coll I.

We also carried out IF analysis of the printed spots (Fig. 4). IF showed a concentration dependent increase in staining intensity of the spots as expected and a homogenous distribution of the fluorescence signal. IF staining against Coll I in spots printed with combined Coll I and BMP 2 showed a small decrease in fluorescence intensity compared to the spots printed without BMP 2 (Fig 4B). This may indicate that competition for epoxy group binding sites may occur when printing at higher protein concentrations.

3.2. MSC attachment on microarray

Rat MSCs were seeded and incubated on the array for 30 min at 37 °C and 5% CO_2. In that timeframe, the cells adhered within the bounds of printed spots, but not in between the spots, due to the A-PEG passivation. Non-adherent cells were then removed by washing the arrays in DMEM. A cell density of 15,000 cells/cm^2

was used, since at higher cell densities, the spot pattern on the chip was overgrown with cells within 5 days. We tested the MSC response to three GF/ECM proteins formulations; Coll I printed formulation concentrations of 50, 100 and 200 μg/mL, BMP 2 at printed formulation concentrations of 1, 5, 10, 20 and 50 μg/mL and finally, all combinations of BMP 2 and Coll I at the formulation concentrations listed. All printed protein spots in the array were of a diameter of 700–800 μm, which was sufficient to capture between 300 and 900 cells/spot and thus permit paracrine and autocrine cell interactions, an important feature of the MSC microenvironment [46].

We observed that increasing the Coll I printed formulation concentration from 50 μg/mL to 200 μg/mL enhanced MSC adhesion 1.9-fold (Fig. 5). Coll I printed at a concentration of 50 μg/mL was more effective for cell attachment after 30 min incubation compared to BMP 2 printed at the same concentration ($P \leqslant 0.05$). The number of attached cells on the Coll I and BMP 2 printed spots was 375.6 ± 37.3 and 218.6 ± 47.3 cells/spot, respectively. The lower formulation concentrations of BMP 2 tested (1 and 5 μg/mL) did not support long-term attachment of MSC; the few cells that were initially captured on the spots detached within 24 h. For the spots containing both proteins, there was a slight increase in cell attachment on spots printed with higher BMP 2 concentrations (10, 20 and 50 μg/mL), especially when combined with Coll I concentrations of 50 and 100 μg/mL.

3.3. Runx2 expression as an early osteogenic differentiation marker

To investigate the effects of surface-immobilised factors on cell differentiation, the cells were fixed at the end of the differentiation period and stained with fluorescent antibodies against Runx2 (Fig. 6A and B). The Runx2 intensity normalised on a per cell basis was used to define a quantitative measure of differentiation towards osteogenic fate on each spot (Fig. 6C). Runx2 intensity increased as the Coll I concentration was elevated from 50 to 200 μg/mL (Fig. 6A), resulting in a 1.5-fold increase across the differentiating MSC population (Fig. 6C).

Runx2 intensity on the spots also rose with increasing printed BMP 2 concentration (Fig. 6A and B) and normalised Runx2 expression levels were elevated almost 2.5 times by printing BMP 2 at 50 μg/mL concentration compared to spots printed at 10 μg/mL concentration ($P \leqslant 0.05$) (Fig. 6C).

When we assessed MSC differentiation towards osteogenic lineages following simultaneous exposure to different ratios of immobilised Coll I and BMP 2, we observed that the level of Runx2 expressed by MSCs cultured on the spots containing 20 μg/mL BMP 2 together with Coll I was almost three times higher than Runx2 expression on spots printed with equivalent concentrations of Coll I alone (Fig. 6C). The maximum normalised Runx2 expression after 6 days of culture was achieved on the spots containing 200 μg/mL Coll I and 20 μg/mL BMP 2 ($P \leqslant 0.05$). A further increase in BMP 2 concentration did not change the Runx2 staining intensity significantly.

3.4. Individual cell analysis of Runx2 expression

The ability to measure expressed markers in individual cells using automated high throughput microscopy allowed us to profile individual cell responses, revealing heterogeneity in greater detail than possible for the normalised analysis above. To represent the extent of osteogenic differentiation in single cells, we defined a 'differentiation space' spanned by the intensity of Runx2 staining in each cell [47,48]. The variation in Runx2 intensity (illustrated in histogram form in Fig. 7 and as box-and-whisker plots in ESI† Fig. S6) within the MSC population was noted to be influenced by the concentration of the printed Coll I solution. Compared to a low Coll I concentration of 50 μg/mL, where the histogram was broad, indicating a more heterogeneous population in terms of the level of Runx2 expression, the higher Coll I concentration of 200 μg/mL induced an increase in the proportion of cells expressing Runx2. Variation in Runx2 expression was also decreased by co-immobilising Coll I and BMP 2 when the BMP 2 concentration exceeded 5 μg/mL. The exposure of cells to the combination of proteins significantly elevated the proportion of cells expressing high levels Runx2 intensity, which suggests an effective stimulation towards osteogenic lineages.

BMP 2 immobilised alone also affected osteogenic differentiation, however at low concentrations of printed BMP 2 in the

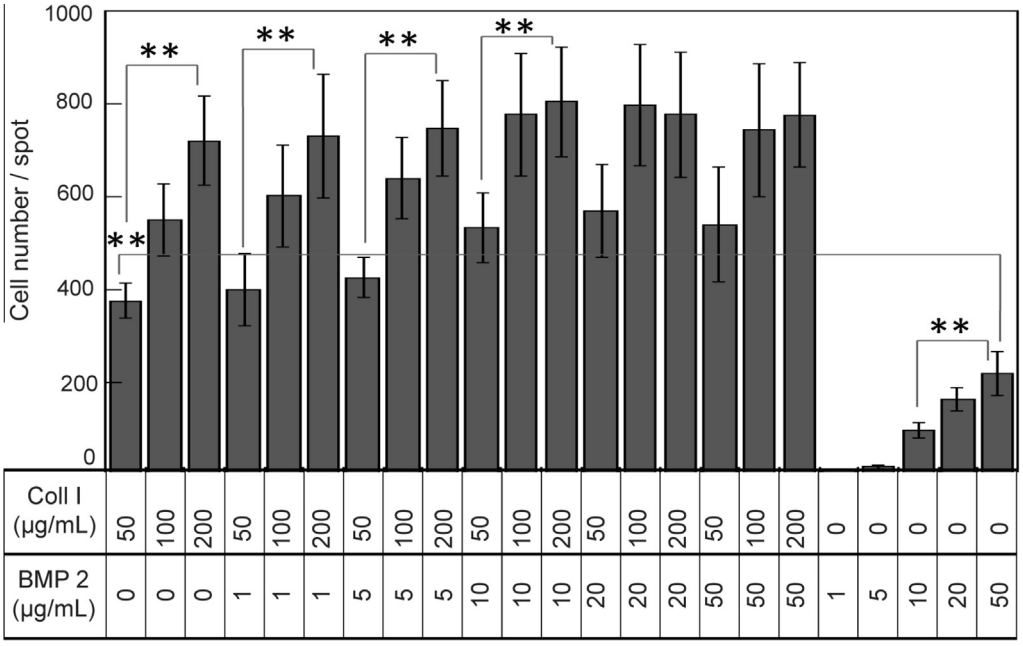

Fig. 5. Average MSC adhesion on Coll I and BMP 2 protein spots printed at various formulation concentrations after 30 min incubation time. Cell seeding density was 15,000 cells/cm^2. Error bars show standard error of cell counts. $n = 3$, $P \leqslant 0.05$.

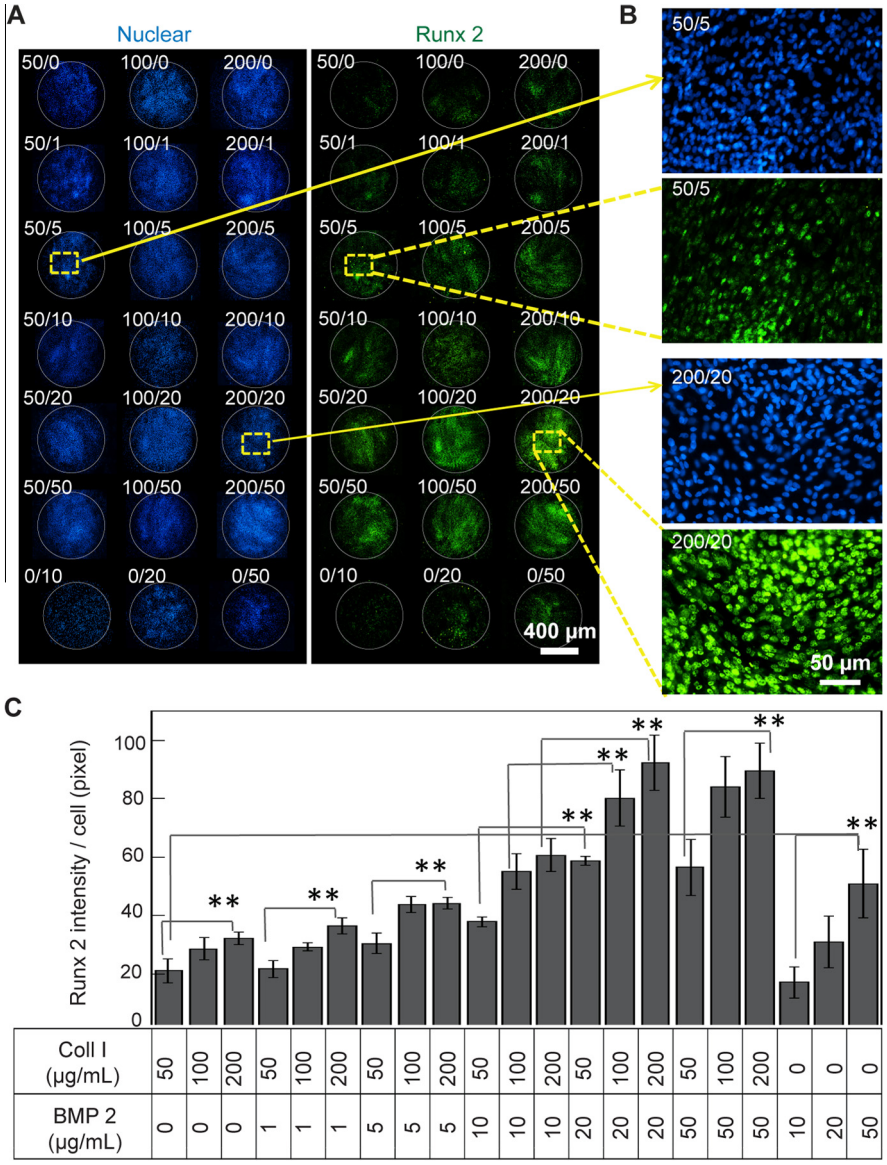

Fig. 6. Characterisation of MSC culture (6 days) on microarrayed spots printed using formulation concentrations of Coll I (0, 50, 100 and 200 μg/mL) and BMP 2 (0, 1, 5, 10, 20 and 50 μg/mL): (A) MSCs stained positively for Runx2 (green) and nuclei were stained with Hoechst 33342 (blue). The seeding density was 15,000 cells/cm^2. Images were taken after 6 days in culture. Scale bar is 400 μm. (B) 20× magnification of a single spot. Scale bar is 50 μm. (C) Runx2 intensity on each spot was analysed by automated high throughput microscopy. The data were normalised to cell number. Error bars correspond to standard error measurement ($n = 3$). Numbers on each image show the printed formulation concentrations of Coll I/BMP 2 (μg/mL). $^{**}P \leqslant 0.05$. (For interpretation of the references to colour in this figure legend, the reader is referred to the web version of this article.)

absence of Coll I, cell attachment to the printed spots was transient and did not permit quantification of Runx2 expression. Increasing the BMP 2 concentration to 50 μg/mL resulted a rise in Runx2 intensity and narrower distribution compared to cells on spots printed with lower BMP 2 concentrations. The variation in Runx2 expression was decreased by co-immobilising Coll I and BMP 2 when BMP 2 concentration exceeded 5 μg/mL (Fig. 7 and ESI† Fig. S6).

Examination of the truncated box plots (ESI† Fig. S6D) indicated that the median Runx2 expression increased almost linearly with Coll I concentration when BMP 2 concentration was held constant. In contrast, Runx2 expression showed a sigmoidal trend when BMP 2 concentration was varied whilst Coll I concentration was held constant (ESI† Fig. S6C). A statistical model was constructed to interrogate the influence of interactions between Coll I and BMP 2 printing concentration in determining Runx2 expression in the MSC population (see Section 2.6 for details). According to this model, BMP 2 and Coll I indeed synergise to upregulate Runx2 expression. The model identifies, within the combinatorial space tested, an optimal BMP 2 printed formulation concentration at around 35 μg/mL (Fig. 8).

3.5. Calcium phosphate deposition as a late stage osteogenic differentiation marker

To assess the ability of surface-immobilised Coll I and BMP 2 to support MSC differentiation to osteoblasts, MSCs were cultured on a Coll I and BMP 2 printed spots for 21 days in the presence of osteoinductive media. Calcium phosphate deposits were stained with Calcein Blue, indicating the extent of mineralisation by osteogenic MSCs (Fig. 9A). The total area of deposited calcium phosphate (which is marked in Fig. 1C) on each printed spot was evaluated after Calcein Blue staining using the software of the high throughput microscope.

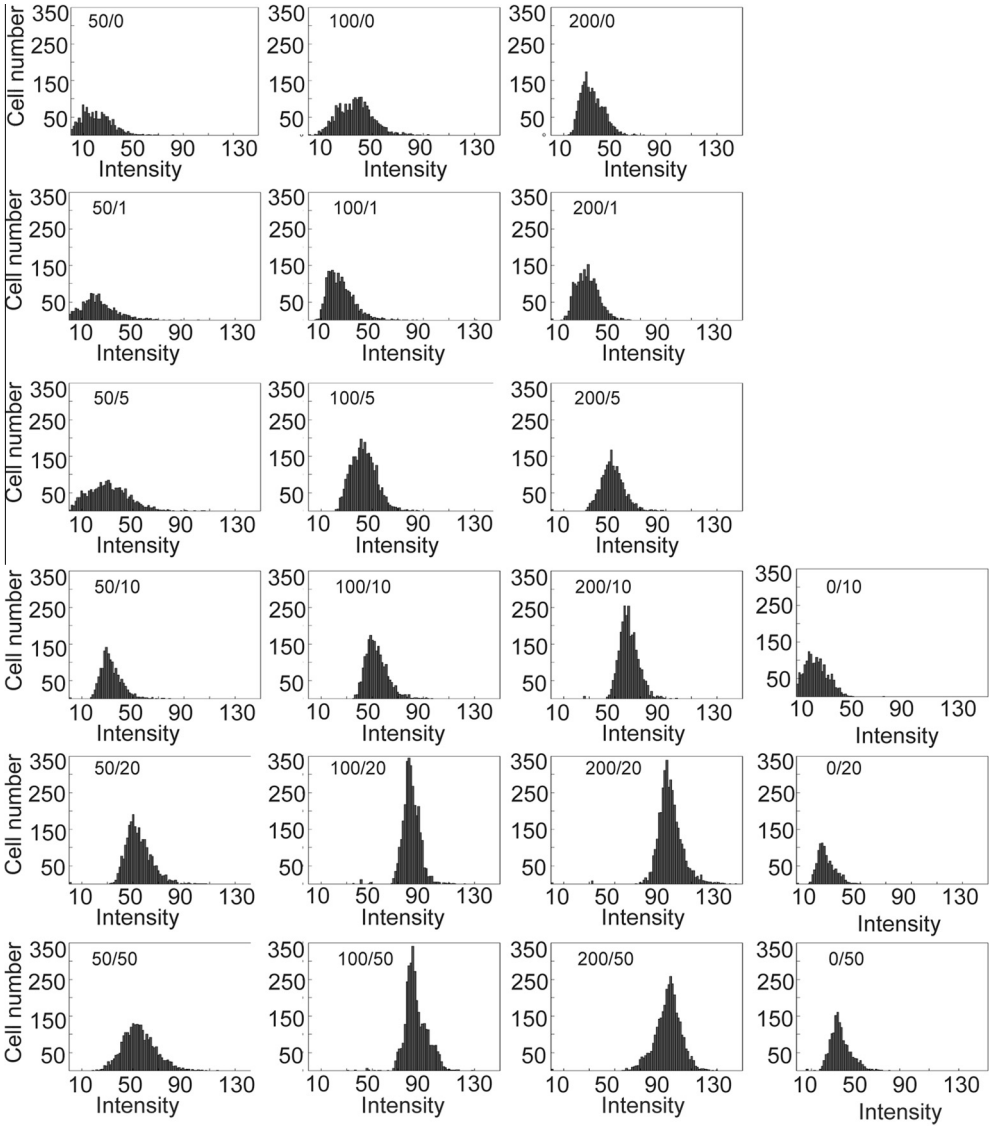

Fig. 7. Runx2 intensity histograms were identified on the protein arrayed spots using automated high throughput microscope. For cell counting purposes, each nucleus (stained with Hoechst 33342) was detected as an object representing a cell. Runx2 intensity was evaluated by Harmony software for each cell. Numbers on each image show the printed formulation concentrations of Coll I/BMP 2 (μg/mL).

For spots containing only Coll I or only BMP 2, we observed that increasing concentrations of printed protein led to an increase in the calcium phosphate deposition area (Fig. 9B). The measured area of calcium phosphate deposition rose from 156.9 to 227.6 μm^2/cell when Coll I concentration was increased from 50 to 200 μg/mL ($P \leqslant 0.05$), indicating the pronounced effect of surface density of immobilised protein on the cell fate. This result was in line with the early stage differentiation results shown in Fig. 6. Similarly, for BMP 2 calcium phosphate deposited area increased from 135 to 320 μm^2/cell when the printed protein concentration was increased from 10 to 50 μg/mL. Comparing calcium phosphate deposition of MSCs cultured on Coll I printed spots at solution concentration of 50 μg/mL and BMP 2 at 50 μg/mL spots showed significantly higher deposition on BMP 2 spots ($P \leqslant 0.05$).

Interestingly, when calcium phosphate deposition was investigated on the printed spots including both Coll I and BMP 2, a 2–3-fold (from 225 to 685 μm^2/cell) increase in calcium phosphate deposition was observed. The maximum calcium phosphate deposited area measured was 682 μm^2/cell when BMP 2 was printed at a concentration of 20 μg/mL with Coll I at a concentration of 200 μg/mL or more. No further significant increase over this level was gained by printing BMP 2 at a higher concentration of 50 μg/mL BMP 2. When BMP 2 was printed at the highest test concentration of 50 μg/mL together with the lowest tested concentration of Coll I (50 μg/mL), the synergistic effect of the GF was less obvious and the calcium phosphate deposited area did not exceed 335 μm^2/cell.

The influence of spot composition on calcium phosphate deposition was further confirmed using Alizarin Red staining (ESI† Fig. S7). This dye is widely used as an indicator of mineralisation [49,50]. On staining of the cultured cells on the printed spots with Alizarin Red, a clearly stained mineralised layer was evident. Intense staining reflects the high amount of calcium phosphate deposited by the cells. The amount of deposited calcium phosphate stained with Alizarin Red followed a similar pattern to that observed for Calcein Blue staining.

4. Discussion

In this study, we have compared the effect of the covalently immobilised BMP 2 in combination with Coll I on the

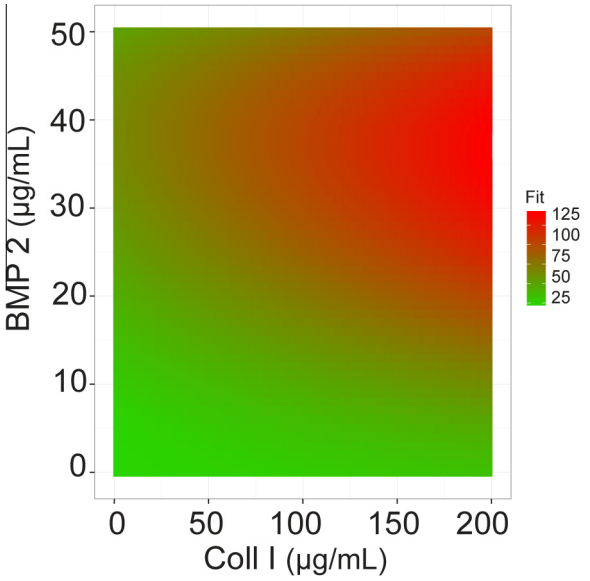

Fig. 8. Heatmap of Runx2 expression: the data were evaluated using high throughput screening of Runx2 based on the model presented in Fig. S2D. Red shows an increased Runx2 expression and green shows a reduced expression. (For interpretation of the references to colour in this figure legend, the reader is referred to the web version of this article.)

differentiation of MSCs along the osteogenic lineage. We used a protein microarray platforms with long-term stability [3]. Each spot was printed using a defined solution of Coll I and/or BMP2. The presence of these immobilised factors on the surface was confirmed by ToF-SIMS analysis and IF results. Both surface analytical techniques illustrated the expected differences in density of immobilised biomolecules on the surface (Fig. 4 and ESI† Fig. S5). The surface density of immobilised biomolecules across the microarray appeared consistent for each test solution concentration. However, defining the immobilised biomolecular density on the surface is challenging. Both ToF-SIMS and IF are semi-quantitative due to matrix effects which are related to biomolecular composition and structure [51].

The attachment of MSCs was investigated on spots printed with different printed formulation concentrations of Coll I and BMP 2. Cell attachment was dependent on the identity of the printed proteins and also the solution concentration used for printing. Both Coll I and BMP 2 were shown to facilitate cell capture, correlating with other studies [3,8,52–54]. On spots printed with low protein content formulations, cell attachment was observed to be poor. MSC attachment improved when protein concentration in the printed formulation was increased. This may be explained by the additional epoxy functional groups able to bind A-PEG within these spots (ESI† Fig. S5). Increasing A-PEG density on the surface resulted in decreasing cell attachment since PEG is known to resist cell attachment [55–57]. Cell density is known to regulate MSC osteogenic differentiation through the competitive influences of cell spreading (via cytoskeletal tension) and intercellular contact [58]. The increased cell–cell contact achieved on spots printed at high Coll I and BMP 2 formulations would be predicted to promote osteogenesis [58,59]. However, low seeding densities have been associated with upregulation of osteogenesis when MSC are cultured under neutral conditions, suggesting that the increased area available for cell spreading on low adhesion spots may also be advantageous [58]. Notably, the spacing of integrin binding ligands

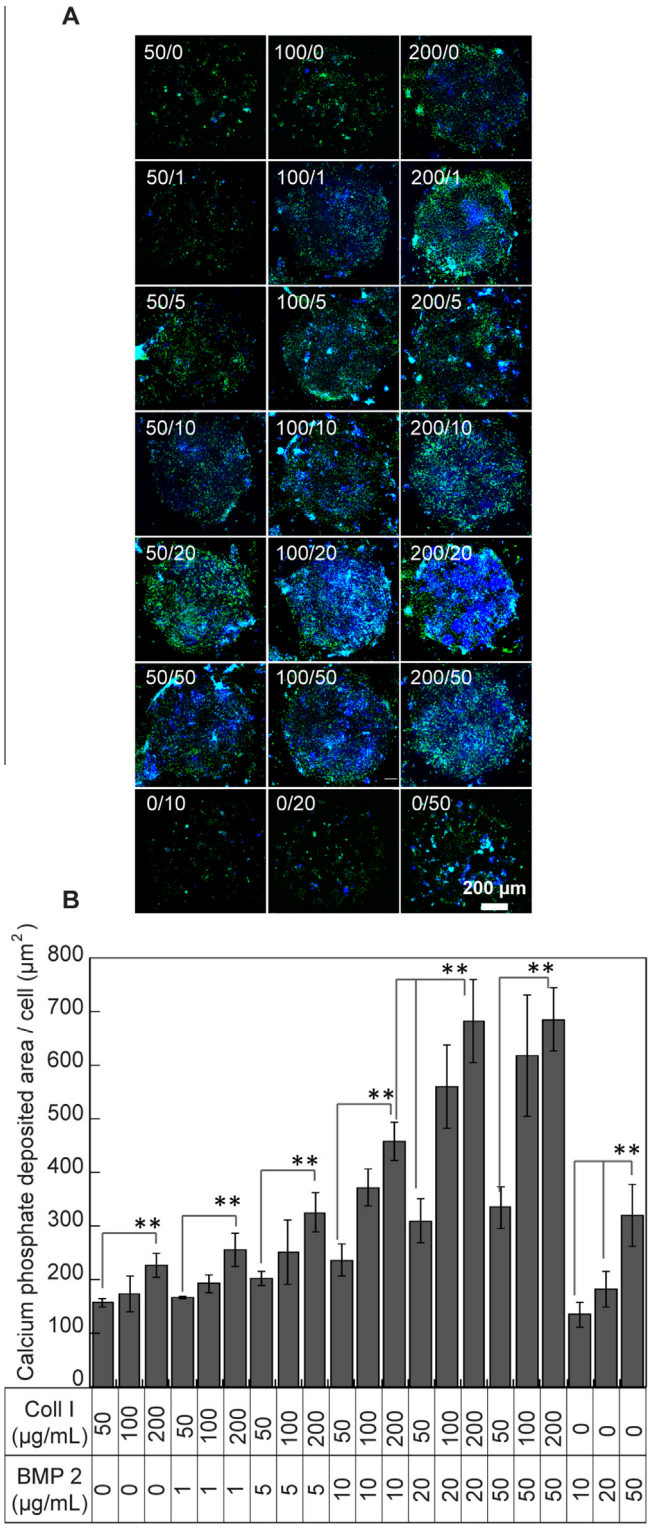

Fig. 9. Evaluation of deposited calcium phosphate: (A) MSCs were seeded on Coll I and BMP 2 printed spots at a seeding density of 15,000 cells/cm^2. After 3 weeks in culture, calcium phosphate mineral nodules were stained by Calcein Blue (blue) and nuclei were stained with PicoGreen (green). (B) Calcium phosphate deposited area (µm^2) was quantified using the automated high throughput microscope. Error bars correspond to standard error measurement. $n = 3$. Numbers on each image show the printed formulation concentrations of Coll I/BMP 2 (µg/mL). (For interpretation of the references to colour in this figure legend, the reader is referred to the web version of this article.)

that govern cell-substrate adhesion is known to control MSC differentiation: sparser immobilisation of RGD peptide on the culture surface results in greater osteoblast formation [14,60,61]. This contrasts with our observation that osteogenic differentiation increases when integrin binding Coll I is printed at high formulation concentrations, emphasising the strong osteogenic stimuli provided by Coll I.

To investigate the combined effects of Coll I stimulation and immobilised BMP 2 on osteoblast differentiation and mineralisation, Runx2 expression and calcium deposition were evaluated. Runx2 is a marker of early stage osteoblast differentiation [31,48], and also contributes to the regulation of skeletal gene expression [62–64]. As shown in Figs. 6 and 9, Coll I and BMP 2 printed together at solution concentrations of 100–200 μg/mL and 20–50 μg/mL, respectively, increased Runx2 expression and calcium phosphate deposition to maximum levels. Analysis via the multiple regression model revealed that the interaction terms between BMP 2 and Coll I concentration components were positive, indicating synergistic enhancement of Runx2 expression when MSC were subjected to these two protein stimuli simultaneously.

Increased expression of Runx2 by cells bound to Coll I and BMP 2 has been observed in previous studies [10,18,48,49,65,66]. Coll I has been described to prompt calcification of the stromal cell matrix after three weeks of MSC culture, suggesting that contact with ECM proteins alone stimulates differentiation [8], This is in line with reports showing that MSCs undergo osteoblast differentiation when in contact with collagen-containing ECM proteins in both *in vitro* and *in vivo* settings [9,67]. Functionalisation of surfaces with BMP 2 has also been shown to induce extensive calcium phosphate deposition, indicating that BMP 2 enhances osteogenic differentiation [29,49], which is consistent with our findings. Here, it has been shown that the combination of BMP 2 and Coll I, in addition to increasing Runx2 expression, also resulted in higher levels of mineralisation at later timepoints. The co-operation of BMP 2 and Coll I signalling pathways has been reported in osteoblast differentiation previously [26,68]. The interaction of surface-immobilised BMP 2 with BMP receptor complexes on the cell surface leads to the initiation of intracellular signalling events without internalisation [69,70]. The BMP 2 signal is propagated through Smad 1 by phosphorylation of receptor-regulated Smad proteins 1/5/8, which then in turn bind to Smad 4 to induce osteogenic gene expression [31,71,72]. Binding of collagen to $\alpha 2\beta 1$-integrin on the cell surface produces a complementary signal that increases transcriptional activity of Smad 1 [73]. Changes in the level of gene expression of Runx2 in MSC can then affect late stage differentiation and calcium phosphate deposition [74–76].

The cooperative action of ECM proteins and GFs are known to play an important role *in vivo*, where signalling, differentiation, and other cell activation often take place in relatively restricted compartments containing different signalling factors [46,77]. ECM proteins provide a substrate for cell adhesion similar to what occurs *in vivo*, whilst GFs provide cells with various signals for controlling cell behaviour or even cell death [40,78]. *In vivo*, GFs bind to ECM proteins, limiting their diffusion [46]. Additionally, the action of BMP 2 on osteoblasts is assisted by ECM-derived signals [26,68,73]. Successful induction of bone formation through immobilised molecules has practical implication for treatments that employ collagenous scaffolds to deliver BMP 2 to initiate bone repair. Immobilisation eliminates diffusion of BMP 2, implicated in ectopic bone formation away from the site of BMP 2 treatment [6,79]. The retention of GF activity after covalent immobilisation to a surface has been demonstrated for a number of other growth factors besides BMP 2 [80–82]. It is likely that the combined action of immobilised ECM proteins and GFs observed here likewise holds true for other ECM/GF mixtures [10,83]. Together, this implies that synergistic interactions between Coll I and BMP 2 occur from early stages of MSC commitment right through to mineralisation. The impact of the synergy may not be confined to one stage of differentiation, but may be propagated through the entire process of differentiation.

5. Conclusions

The rational design of bioactive tissue engineered scaffolds for directing bone regeneration requires a comprehensive knowledge of cell interactions with the immobilised biomolecules. In this study, we employed cell microarrays of immobilised Coll I and BMP 2 to determine an optimal factor combination to support MSC differentiation towards the osteogenic lineage. During the first week of differentiation, Runx2 expression in MSC was observed to increase with the printed formulation concentration of BMP 2 and Coll I. The co-operation of BMP 2 and Coll I in the induction of Runx2 expression was evident where the two proteins were printed together. Employing a statistical model to analyse single cell protein expression, the interaction between Coll I and BMP 2 was determined to be synergistic. Optimal surface conditions for Runx2 expression also produced an increase in mineralisation later in MSC differentiation. Together, our results indicate that a combination of both Coll I and BMP 2 further enhance osteogenesis of MSCs synergistically above the level of the individual proteins. Our proof-of-principle results demonstrate that our multi-protein microarray approach, in combination with automated image acquisition and quantitative, multi-parameter analysis of cellular responses can underpin the design and rapid construction of advanced biomaterials and scaffolds.

Acknowledgment

This research was conducted and funded by the Australian Research Council Centre of Excellence in Convergent Bio-Nano Science and Technology (Project No. CE140100036).

Appendix A. Supplementary data

Supplementary data associated with this article can be found, in the online version, at http://dx.doi.org/10.1016/j.actbio.2015.07.027.

References

[1] D.M. Titmarsh, H. Chen, E.J. Wolvetang, J.J. Cooper-White, Arrayed cellular environments for stem cells and regenerative medicine, Biotechnol. J. 8 (2012) 167–179.
[2] X. Yao, R. Peng, J. Ding, Cell-material interactions revealed via material techniques of surface patterning, Adv. Mater. 25 (2013) 5257–5286.
[3] S. Rasi Ghaemi, F. Harding, B. Delalat, R. Vasani, N.H. Voelcker, Surface engineering for long-term culturing of mesenchymal stem cell microarrays, Biomacromolecules 14 (2013) 2675–2683.
[4] T.-C. Tseng, S.-h. Hsu, Substrate-mediated nanoparticle/gene delivery to MSC spheroids and their applications in peripheral nerve regeneration, Biomaterials 35 (2014) 2630–2641.
[5] M. Maumus, C. Jorgensen, D. Noël, Mesenchymal stem cells in regenerative medicine applied to rheumatic diseases: role of secretome and exosomes, Biochimie 95 (2013) 2229–2234.
[6] J. Bashir, A. Sherman, H. Lee, L. Kaplan, J.M. Hare, Mesenchymal stem cell therapies in the treatment of musculoskeletal diseases, Am. J. Phys. Med. Rehabil. 6 (2014) 61–69.
[7] L. Wang, Y. Huang, K. Pan, X. Jiang, C. Liu, Osteogenic responses to different concentrations/ratios of bmp-2 and bfgf in bone formation, Ann. Biomed. Eng. 38 (2010) 77–87.
[8] R.M. Salasznyk, W.A. Williams, A. Boskey, A. Batorsky, G.E. Plopper, Adhesion to vitronectin and collagen i promotes osteogenic differentiation of human mesenchymal stem cells, J. Biomed. Biotechnol. 1 (2004) 24–34.
[9] Y.J. Choi, J.Y. Lee, C.P. Chung, Y.J. Park, Enhanced osteogenesis by collagen-binding peptide from bone sialoprotein in vitro and in vivo, J. Biomed. Mater. Res. A101A (2013) 547–554.

[10] X. Zhang, W.-G. Guo, H. Cui, H.-Y. Liu, Y. Zhang, W.E.G. Müller, et al., In vitro and in vivo enhancement of osteogenic capacity in a synthetic BMP-2 derived peptide-coated mineralized collagen composite, J. Tissue Eng. Regener. Med. (2013) 1–9.

[11] P.-Y. Wang, W.-B. Tsai, N.H. Voelcker, Screening of rat mesenchymal stem cell behaviour on polydimethylsiloxane stiffness gradients, Acta Biomater. 8 (2012) 519–530.

[12] P.-Y. Wang, L.R. Clements, H. Thissen, A. Jane, W.-B. Tsai, N.H. Voelcker, Screening mesenchymal stem cell attachment and differentiation on porous silicon gradients, Adv. Funct. Mater. (2012) 1–10.

[13] X. Yao, R. Peng, J. Ding, Effects of aspect ratios of stem cells on lineage commitments with and without induction media, Biomaterials 34 (2013) 930–939.

[14] X. Wang, C. Yan, K. Ye, Y. He, Z. Li, J. Ding, Effect of RGD nanospacing on differentiation of stem cells, Biomaterials 34 (2013) 2865–2874.

[15] L.V. Logovskaya, T.B. Bukharova, A.V. Volkov, E.B. Vikhrova, O.V. Makhnach, D.V. Goldshtein, Induction of osteogenic differentiation of multipotent mesenchymal stromal cells from human adipose tissue, Bull. Exp. Biol. Med. 155 (2013) 145–150.

[16] X. Ma, X. Zhang, Y. Jia, S. Zu, S. Han, D. Xiao, et al., Dexamethasone induces osteogenesis via regulation of hedgehog signalling molecules in rat mesenchymal stem cells, Int. Orthop. 37 (2013) 1399–1404.

[17] P. Yilgor, K. Tuzlakoglu, R.L. Reis, N. Hasirci, V. Hasirci, Incorporation of a sequential BMP-2/BMP-7 delivery system into chitosan-based scaffolds for bone tissue engineering, Biomaterials 30 (2009) 3551–3559.

[18] F.R. Kloss, S. Singh, O. Hächl, J. Rentenberger, T. Auberger, A. Kraft, et al., BMP-2 immobilized on nanocrystalline diamond-coated titanium screws; demonstration of osteoinductive properties in irradiated bone, Head Neck 35 (2013) 235–241.

[19] J.R. Overman, E. Farré-Guasch, M.N. Helder, C.M. ten Bruggenkate, E.A. Schulten, J. Klein-Nulend, Short (15 minutes) bone morphogenetic protein-2 treatment stimulates osteogenic differentiation of human adipose stem cells seeded on calcium phosphate scaffolds in vitro, Tissue Eng. A 19 (2013) 571–581.

[20] M. Mizuno, Y. Kuboki, Osteoblast-related gene expression of bone marrow cells during the osteoblastic differentiation induced by type I collagen, Jpn. Biochem. Soc. 129 (2001) 133–138.

[21] D.E. Discher, D.J. Mooney, P.W. Zandstra, Growth factors, matrices, and forces combine and control stem cells, Science 324 (2009) 1673–1677.

[22] S. Cheng, C. Lai, A. Fausto, Regulation of avb3 and avb5 integrins by dexamethasone in normal human osteoblastic cells, J. Cell. Biochem. 77 (2000) 265–276.

[23] A.S. Rowlands, P.A. George, J.J. Cooper-White, Directing osteogenic and myogenic differentiation of MSCs: interplay of stiffness and adhesive ligand presentation, Am. J. Physiol. Cell Physiol. 295 (2008) C1037–C1044.

[24] D. Wahl, E. Sachlos, C. Liu, J. Czernuszka, Controlling the processing of collagen-hydroxyapatite scaffolds for bone tissue engineering, J. Mater. Sci.: Mater. Med. 18 (2007) 201–209.

[25] L.R. Clements, P.-Y. Wang, F. Harding, W.-B. Tsai, H. Thissen, N.H. Voelcker, Mesenchymal stem cell attachment to peptide density gradients on porous silicon generated by electrografting, Phys. Status Solidi A (2010) 1–6.

[26] G. Xiao, R. Gopalakrishnan, D. Jiang, E. Reith, M.D. Benson, R.T. Franceschi, Bone morphogenetic proteins, extracellular matrix, and mitogen-activated protein kinase signaling pathways are required for osteoblast-specific gene expression and differentiation in MC3T3-E1 cells, J. Bone Miner. Res. 17 (2002) 101–110.

[27] D. Zimmerman, F. Jin, P. Leboy, S. Hardy, C. Damsky, Impaired bone formation in transgenic mice resulting from altered integrin function in osteoblasts, Dev. Biol. 220 (2000) 2–15.

[28] K.C. Clause, T.H. Barker, Extracellular matrix signaling in morphogenesis and repair, Curr. Opin. Biotechnol. 24 (2013) 830–833.

[29] R. Budiraharjo, K.G. Neoh, E.-T. Kang, Enhancing bioactivity of chitosan film for osteogenesis and wound healing by covalent immobilization of BMP-2 or FGF-2, J. Biomater. Sci. Polym. Ed. 24 (2012) 645–662.

[30] M. Geiger, R.H. Li, W. Friess, Collagen sponges for bone regeneration with rhBMP-2, Adv. Drug Deliv. Rev. 55 (2003) 1613–1629.

[31] T. Matsubara, K. Kida, A. Yamaguchi, K. Hata, F. Ichida, H. Meguro, et al., BMP2 regulates osterix through msx2 and runx2 during osteoblast differentiation, J. Biol. Chem. 283 (2008) 29119–29125.

[32] M. Murata, B.-Z. Huang, T. Shibata, S. Imai, N. Nagai, M. Arisue, Bone augmentation by recombinant human BMP-2 and collagen on adult rat parietal bone, Int. J. Oral Maxillofac. Surg. 28 (1999) 232–237.

[33] C.M. Halliwell, A.E.G. Cass, A factorial analysis of silanization conditions for the immobilization of oligonucleotides on glass surfaces, Anal. Chem. 73 (2001) 2476–2483.

[34] S.A. Rodríguez-Seguí, M. Pla-Roca, E. Engel, J.A. Planell, E. Martínez, J. Samitier, Influence of fabrication parameters in cellular microarrays for stem cell studies, Mater. Sci. 20 (2009) 1525–1533.

[35] M.S. Wagnera, D.G. Castner, Analysis of adsorbed proteins by static time-of-flight secondary ion mass spectrometry, Appl. Surf. Sci. 231–232 (2004) 366–376.

[36] B.-A. Gotliv, A. Veis, Peritubular dentin, a vertebrate apatitic mineralized tissue without collagen: role of a phospholipid–proteolipid complex, Calcif. Tissue Int. 81 (2007) 191–205.

[37] M. Glassner, K.K. Oehlenschlaeger, A. Welle, M. Bruns, C. Barner-Kowollik, Polymer surface patterning via Diels–Alder trapping of photo-generated thioaldehydes, Chem. Commun. 49 (2013) 633–635.

[38] H.K. Shon, J.G. Son, K.-B. Lee, J. Kim, M.S. Kim, I.S. Choi, et al., Chemical imaging analysis of the micropatterns of proteins and cells using cluster ion beam-based time-of-flight secondary ion mass spectrometry and principal component analysis, Bull. Korean Chem. Soc. 34 (2013) 815–819.

[39] L.R. Clements, P.-Y. Wang, W.-B. Tsai, H. Thissen, N.H. Voelcker, Electrochemistry-enabled fabrication of orthogonal nanotopography and surface chemistry gradients for high-throughput screening, Lab Chip 12 (2012) 1480–1486.

[40] K. Crapnell, R. Blaesius, A. Hastings, D.P. Lennon, A.I. Caplan, S.P. Bruder, Growth, differentiation capacity, and function of mesenchymal stem cells expanded in serum-free medium developed via combinatorial screening, Exp. Cell Res. 319 (2013) 1409–1418.

[41] C.P. Ng, A.R. Mohamed Sharif, D.E. Heath, J.W. Chow, C.B.Y. Zhang, M.B. Chan-Park, et al., Enhanced ex vivo expansion of adult mesenchymal stem cells by fetal mesenchymal stem cell ECM, Biomaterials 35 (2014) 4046–4057.

[42] M. Veith, C. Dufloux, S. Rasi Ghaemi, C. Aktas, N. Voelcker, Gradients of Al/Al_2O_3 nanostructures for screening mesenchymal stem cell proliferation and differentiation, Open J. Regener. Med. 3 (2013) 74–79.

[43] M.S. Wagner, D.G. Castner, Characterization of adsorbed protein films by time-of-flight secondary ion mass spectrometry with principal component analysis, Langmuir 17 (2001) 4649–4660.

[44] W.N. Venables, B.D. Ripley, Modern Applied Statistics with R, fourth ed., Springer, New York, 2002.

[45] A.J. Urquhart, D.G. Anderson, M. Taylor, M.R. Alexander, R. Langer, M.C. Davies, High throughput surface characterisation of a combinatorial material library, Adv. Mater. 19 (2007) 2486–2491.

[46] S. Rasi Ghaemi, F.J. Harding, B. Delalat, S. Gronthos, N.H. Voelcker, Exploring the mesenchymal stem cell niche using high throughput screening, Biomaterials 34 (2013) 7601–7615.

[47] C.A. Gersbach, B.A. Byers, G.K. Pavlath, R.E. Guldberg, A.J. García, Runx2/Cbfa1-genetically engineered skeletal myoblasts mineralize collagen scaffolds in vitro, Biotechnol. Bioeng. 88 (2004) 369–378.

[48] R.T. Franceschi, G. Xiao, Regulation of the osteoblast-specific transcription factor, Runx2: responsiveness to multiple signal transduction pathways, J. Cell. Biochem. 88 (2003) 446–454.

[49] M.-J. Kim, B. Lee, K. Yang, J. Park, S. Jeon, S.H. Um, et al., BMP-2 peptide-functionalized nanopatterned substrates for enhanced osteogenic differentiation of human mesenchymal stem cells, Biomaterials 34 (2013) 7236–7246.

[50] N. Maegawa, K. Kawamura, M. Hirose, H. Yajima, Y. Takakura, H. Ohgushi, Enhancement of osteoblastic differentiation of mesenchymal stromal cells cultured by selective combination of bone morphogenetic protein-2 (BMP-2) and fibroblast growth factor-2 (FGF-2), J. Tissue Eng. Regener. Med. 1 (2007) 306–313.

[51] M.S. Lee, Mass Spectrometry Handbook, John Wiley & Sons, Hoboken, New Jersey, 2012.

[52] S.M. Shiels, K.D. Solomon, M. Pilia, M.R. Appleford, J.L. Ong, BMP-2 tethered hydroxyapatite for bone tissue regeneration: coating chemistry and osteoblast attachment, J. Biomed. Mater. Res. A100A (2012) 3117–3123.

[53] I.-K. Lee, I.-H. Han, S.-W. Hwang, J.-J. Ryu, Analysis of attachment, proliferation and differentiation response of human mesenchymal stem cell to various implant surfaces coated with rhBMP-2, J. Korean Acad. Prosthod. 50 (2012) 44–52.

[54] P.-Y. Wang, T.-H. Wu, P.-H.G. Chao, W.-H. Kuo, M.-J. Wang, C.-C. Hsu, et al., Modulation of cell attachment and collagen production of anterior cruciate ligament cells via submicron grooves/ridges structures with different cell affinity, Biotechnol. Bioeng. 110 (2013) 327–337.

[55] M. Sun, J. Deng, Z. Tang, J. Wu, D. Li, H. Chen, et al., A correlation study of protein adsorption and cell behaviors on substrates with different densities of PEG chains, Colloid Surf. B: Biointerfaces 122 (2014) 134–142.

[56] D.E. Heath, A.R.M. Sharif, C. Ping Ng, M.G. Rhoads, L.G. Griffith, P.T. Hammond, et al., Regenerating the cell resistance of micromolded PEG hydrogels, Lab Chip 15 (2015) 2073–2089.

[57] Y. Dang, M. Quan, C.-M. Xing, Y.-B. Wang, Y.-K. Gong, Biocompatible and antifouling coating of cell membrane phosphorylcholine and mussel catechol modified multi-arm PEGs, J. Mater. Chem. B 3 (2015) 2350–2361.

[58] R. Peng, X. Yao, B. Cao, J. Tang, J. Ding, The effect of culture conditions on the adipogenic and osteogenic inductions of mesenchymal stem cells on micropatterned surfaces, Biomaterials 33 (2012) 6008–6019.

[59] J. Tang, R. Peng, J. Ding, The regulation of stem cell differentiation by cell–cell contact on micropatterned material surfaces, Biomaterials 31 (2010) 2470–2476.

[60] K. Ye, X. Wang, L. Cao, S. Li, Z. Li, L. Yu, et al., Matrix stiffness and nanoscale spatial organization of cell-adhesive ligands direct stem cell fate, Nano Lett. (2015), http://dx.doi.org/10.1021/acs.nanolett.5b01619.

[61] X. Wang, S. Li, C. Yan, P. Liu, J. Ding, Fabrication of RGD micro/nanopattern and corresponding study of stem cell differentiation, Nano Lett. 15 (2015) 1457–1467.

[62] J.-J. Sun, X.-H. Zheng, L.-Y. Wang, L. Liu, W. Jing, Y.-F. Lin, et al., New bone formation enhanced by ADSCs overexpressing hRunx2 during mandibular distraction osteogenesis in osteoporotic rabbits, J. Orthop. Res. 32 (2014) 709–720.

[63] F. Yang, P.-W. Yuan, Y.-Q. Hao, Z.-M. Lu, Emodin enhances osteogenesis and inhibits adipogenesis, BMC Complement. Altern. Med. 14 (2014) 74.

[64] X. Kang, F. Kang, B. Yang, H. Guo, Y. Quan, S. Dong, Micro RNA-451 promoting osteogenesis of mesenchymal stem cells by targeting regulatory calcium binding protein 39, Eur. PMC Labs 27 (2013) 1122–1127.

[65] N. Moore, N. Lin, N. Gallant, M. Becker, Synergistic enhancement of human bone marrow stromal cell proliferation and osteogenic differentiation on BMP-2-derived and RGD peptide concentration gradients, Acta Biomater. 7 (2011) 2091–2100.
[66] K.M. Yamada, S. Even-Ram, Integrin regulation of growth factor receptors, Nat. Cell Biol. 4 (2002) E75–E76.
[67] S. Ichinose, M. Tagami, T. Muneta, H. Mukohyama, I. Sekiya, Comparative sequential morphological analyses during in vitro chondrogenesis and osteogenesis of mesenchymal stem cells embedded in collagen gels, Med. Mol. Morphol. 46 (2013) 24–33.
[68] A. Jikko, S.E. Harris, D. Chen, D.L. Mendrick, C.H. Damsky, Collagen integrin receptors regulate early osteoblast differentiation induced by BMP-2, J. Bone Miner. Res. 14 (1999) 1075–1083.
[69] J. Zhang, K.G. Neoh, X. Hu, E.-T. Kang, W. Wang, Combined effects of direct current stimulation and immobilized BMP-2 for enhancement of osteogenesis, Biotechnol. Bioeng. 110 (2013) 1466–1475.
[70] E.H. Schwab, T.L.M. Pohl, T. Haraszti, G.K. Schwaerzer, C. Hiepen, J.P. Spatz, et al., Nanoscale control of surface immobilized BMP-2: toward a quantitative assessment of BMP-mediated signaling events, Nano Lett. 15 (2015) 1526–1534.
[71] M.Q. Hassan, R.S. Tare, S.H. Lee, M. Mandeville, M.I. Morasso, A. Javed, et al., BMP2 commitment to the osteogenic lineage involves activation of Runx2 by Dlx3 and a homeodomain transcriptional network, J. Biol. Chem. 281 (2006) 40515–40526.
[72] N. Yamamoto, S. Akiyama, T. Katagiri, M. Namiki, T. Kurokawa, T. Suda, Smad1 and smad5 act downstream of intracellular signalings of BMP-2 that inhibits myogenic differentiation and induces osteoblast differentiation in C2C12 myoblasts, Biochem. Biophys. Res. Commun. 238 (1997) 574–580.
[73] M. Suzawa, Y. Tamura, S. Fukumoto, K. Miyazono, T. Fujita, S. Kato, et al., Stimulation of smad1 transcriptional activity by ras-extracellular signal-regulated kinase pathway: a possible mechanism for collagen-dependent osteoblastic differentiation, J. Bone Miner. Res. 17 (2002) 240–248.
[74] S. Yang, D. Wei, D. Wang, M. Phimphilai, P.H. Krebsbach, R.T. Franceschi, In vitro and in vivo synergistic interactions between the Runx2/Cbfa1 transcription factor and bone morphogenetic protein-2 in stimulating osteoblast differentiation, J. Bone Miner. Res. 18 (2003) 705–715.
[75] X. Zhang, M. Yang, L. Lin, P. Chen, K.T. Ma, C.Y. Zhou, et al., Runx2 overexpression enhances osteoblastic differentiation and mineralization in adipose-derived stem cells in vitro and in vivo, Calcif. Tissue Int. 79 (2006) 169–178.
[76] B.A. Byers, A.J. Garcia, Exogenous Runx2 expression enhances in vitro osteoblastic differentiation and mineralization in primary bone marrow stromal cells, Tissue Eng. 10 (2004) 1623–1632.
[77] A. Ramakrishnan, M. Pillai, B. Torok-Storb, The adult stem cell niche, in: K. Turksen (Ed.), Adult Stem Cells, Springer, New York, 2014, pp. 15–30.
[78] L. Yang, Y.S. Roh, J. Song, B. Zhang, C. Liu, R. Loomba, et al., Transforming growth factor beta signaling in hepatocytes participates in steatohepatitis through regulation of cell death and lipid metabolism in mice, Hepatology 59 (2014) 483–495.
[79] P.T. Hamilton, M.S. Jansen, S. Ganesan, R.E. Benson, R. Hyde-DeRuyscher, W.F. Beyer, et al., Improved bone morphogenetic protein-2 retention in an injectable collagen matrix using bifunctional peptides, PLoS One 8 (2013) 70715.
[80] S. Konagaya, K. Kato, T. Nakaji-Hirabayashi, Y. Arima, H. Iwata, Array-based functional screening of growth factors toward optimizing neural stem cell microenvironments, Biomaterials 32 (2011) 5015–5022.
[81] M. Ghaedi, N. Tuleuova, M.A. Zern, J. Wu, A. Revzin, Bottom-up signaling from HGF-containing surfaces promotes hepatic differentiation of mesenchymal stem cells, Biochem. Biophys. Res. Commun. 407 (2011) 295–300.
[82] Y. Soen, A. Mori, T.D. Palmer, P.O. Brown, Exploring the regulation of human neural precursor cell differentiation using arrays of signaling microenvironments, Mol. Syst. Biol. (2006) 1–14.
[83] H. Ao, Y. Xie, H. Tan, X. Wu, G. Liu, A. Qin, et al., Improved hMSC functions on titanium coatings by type I collagen immobilization, J. Biomed. Mater. Res. A 102 (2014) 204–214.